

## Auroral kilometric radiation and magnetosphere-ionosphere coupling process during magnetic storms

T. Seki,<sup>1,2</sup> A. Morioka,<sup>1</sup> Y. S. Miyoshi,<sup>3</sup> F. Tsuchiya,<sup>1</sup> H. Misawa,<sup>1</sup> W. Gonzalez,<sup>4</sup>  
T. Sakanoi,<sup>1</sup> H. Oya,<sup>5</sup> H. Matsumoto,<sup>6</sup> K. Hashimoto,<sup>6</sup> and T. Mukai<sup>2</sup>

Received 6 December 2004; revised 2 February 2005; accepted 11 February 2005; published 14 May 2005.

[1] This paper presents an investigation of a magnetosphere-ionosphere (M-I) coupling process during magnetic storms, using observations of auroral kilometric radiation (AKR) in the field-aligned acceleration region and plasma density variation in the plasma sheet. The main phase electron precipitation, which AKR does not accompany, was confirmed as not characterized by inverted-V type precipitation but rather by precipitation with Maxwellian type distribution. This indicates the absence of the field-aligned potential in the M-I coupling region during the early phase of the magnetic storm. We found that the superdense plasma in the plasma sheet is closely concerned with the AKR activity; that is, the appearance of the superdense plasma sheet seems to suppress the AKR activity. On the basis of these observations we discuss the current-voltage relation between the magnetosphere and ionosphere. The occurrence of the superdense plasma sheet accompanied with the AKR disappearance was found to be caused by coronal mass ejection (CME) with magnetic cloud. The overall story from the arrival of CME at the Earth to the AKR disappearance in the M-I coupling region is presented.

**Citation:** Seki, T., et al. (2005), Auroral kilometric radiation and magnetosphere-ionosphere coupling process during magnetic storms, *J. Geophys. Res.*, 110, A05206, doi:10.1029/2004JA010961.

### 1. Introduction

[2] Auroral kilometric radiation (AKR) has been believed to be a manifestation of field-aligned acceleration above the auroral ionosphere during substorms because electrons beamed down from the field-aligned acceleration region emanate the free-space mode radio waves of AKR as well as excite discrete auroral emissions. The remote observation of AKR from space thus has been utilized to diagnose the structure and dynamics of not only the AKR source region but also the acceleration region.

[3] *Kaiser and Alexander* [1977] discussed AKR source dynamics from the spectral variation of AKR during the substorm growth and expansion phase. Fine structures of AKR that indicate the small source region of the radiation have been studied in terms of the small-scale acceleration region traveling along the auroral field line [*Gurnett et al.*, 1978; *Morioka et al.*, 1981; *Menietti et al.*, 2000; *Pottelette et al.*, 2001]. The fast upward and downward expansion of

AKR source was investigated from the characteristics of impulsive wideband bursts of AKR [*Hanasz et al.*, 2001].

[4] The dynamics of AKR is strongly concerned with magnetosphere-ionosphere (M-I) coupling. *Kasaba et al.* [1997] and *Kumamoto and Oya* [1998] disclosed the difference in development of the acceleration region between summer and winter hemispheres from the statistical study of AKR distribution and pointed out the importance of the plasma density around the M-I coupling region. The seasonal and solar cycle dynamics of the AKR source region was also shown in relation to the plasma condition in the M-I coupling region by *Kumamoto et al.* [2003] and *Green et al.* [2004]. These studies by means of remote AKR observations have contributed to investigation of the coupling between the auroral ionosphere and magnetosphere during substorms.

[5] Recently, *Morioka et al.* [2003] reported unexpected nature of AKR during magnetic storms. Their results were (1) AKR often disappears in the initial and main phases of magnetic storms in spite of the large enhancement of field-aligned currents. (2) At that time, the energy spectra of precipitating electrons do not show signatures of field-aligned acceleration but rather show hot electron enhancement, probably from the plasma sheet. (3) The radiation activates strongly in the recovery phase and (4) AKR tends to disappear in larger storms. These results indicate that the field-aligned electric field is not formed in the early phases of magnetic storms and suggest that the M-I coupling during storms is different from that during usual substorms.

[6] In this paper we investigate the relationship between the AKR disappearance and plasma sheet plasma density

<sup>1</sup>Planetary Plasma and Atmospheric Research Center, Tohoku University, Sendai, Japan.

<sup>2</sup>Institute of Space and Astronautical Science, Japan Aerospace Exploration Agency, Sagami, Japan.

<sup>3</sup>Solar-Terrestrial Environment Laboratory, Nagoya University, Nagoya, Japan.

<sup>4</sup>National Institute of Space Research, São José dos Campos, Brazil.

<sup>5</sup>Fukui University of Technology, Fukui, Japan.

<sup>6</sup>Research Institute for Sustainable Humanosphere, Kyoto University, Kyoto, Japan.

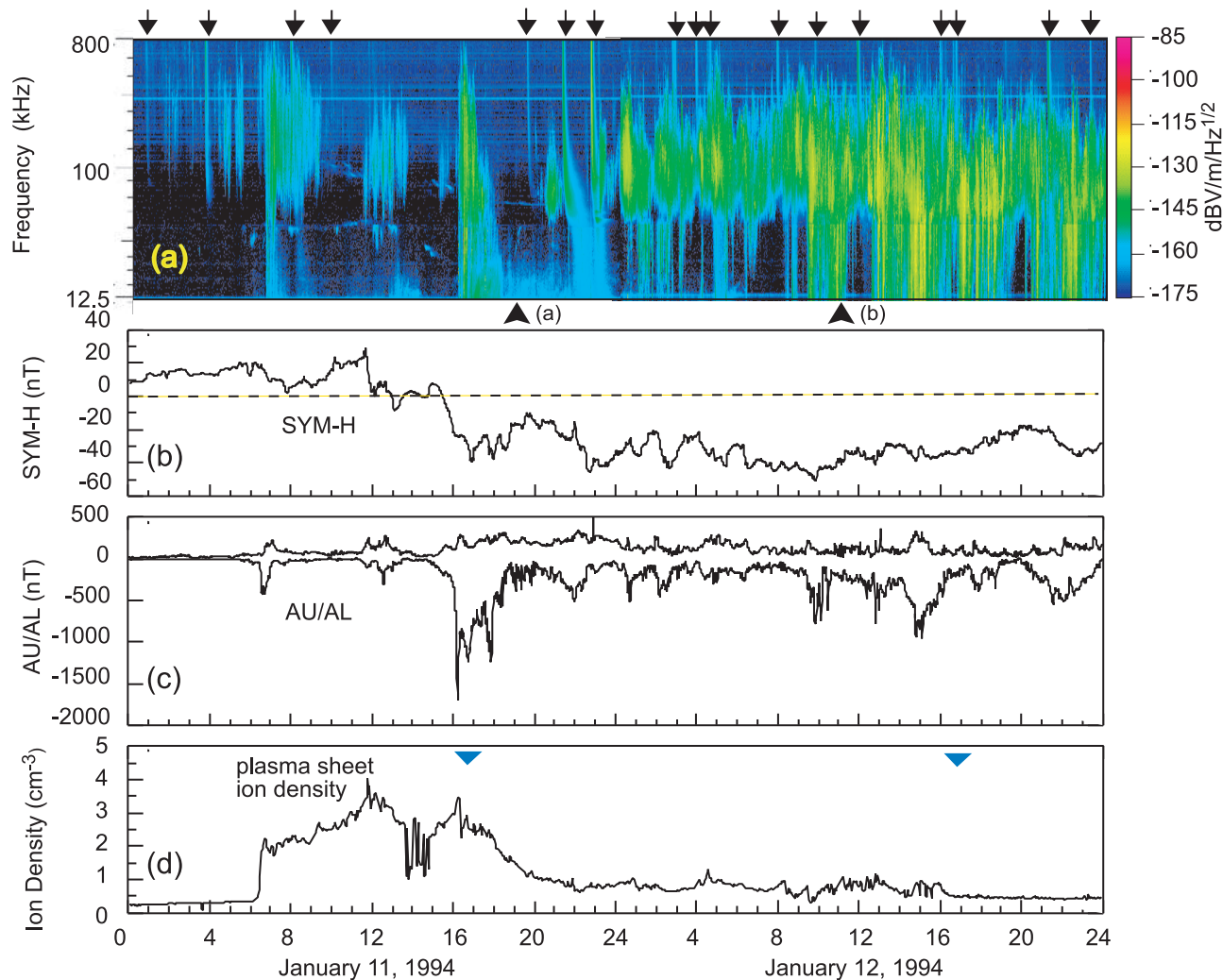


**Figure 1.** Typical example of auroral kilometric radiation (AKR) disappearance during a magnetic storm. (a) The frequency-time ( $f$ - $t$ ) spectrogram of the radio waves in the frequency range from 12.5 to 800 kHz observed by the Geotail satellite on 11–12 January 1994. During the period, Geotail was almost located in the equatorial midnight magnetotail (MLT: 23–24 hours,  $X_{\text{GSM}} = -85$ – $-100 R_E$ ,  $Y_{\text{GSM}} = 10$ – $20 R_E$ ,  $Z_{\text{GSM}} = 10$ – $-5 R_E$ ). The arrows on the top of  $f$ - $t$  spectrogram indicate the solar type III radio bursts. (b) SYM-H index. (c) AU and AL indices. (d) Plasma sheet ion density in the energy range from 130 eV/q to 45 keV/q observed with the MPA on board the 1989-046 geosynchronous satellite. The local midnight of the satellite is indicated by the triangles in Figure 1d.

during magnetic storms to clarify a feature of the storm-time magnetosphere-ionosphere coupling process using remote observations of AKR and in situ observation of the plasma-sheet plasma.

## 2. AKR Disappearance and M-I Coupling

[7] A typical example of AKR disappearance during a magnetic storm is shown in Figure 1. Figure 1a shows the frequency-time ( $f$ - $t$ ) spectrogram of radio wave signals in the frequency range from 12.5 to 800 kHz observed with the Plasma Wave Instrument (PWI) [Matsumoto *et al.*, 1994] on board the Geotail satellite. During the time period indicated in Figure 1, Geotail was almost located in the equatorial midnight magnetotail (MLT: 23–24 hours,  $X_{\text{GSM}} = -85$ – $-100 R_E$ ,  $Y_{\text{GSM}} = 10$ – $20 R_E$ ,  $Z_{\text{GSM}} = 10$ – $-5 R_E$  ( $R_E$ : Earth radii)). The AKR activity was very weak before 0600 UT on

11 January 1994. At around 0600 UT, AKR appeared corresponding to a substorm activity with AL amplitude of  $-400$  nT as seen in Figure 1c. After that, a magnetic storm commenced and descended to the main phase from about 1200 UT, although the start time of the storm is not apparent from the SYM-H index in Figure 1b. Here, we used the SYM-H index to describe the storm activity, which is essentially the same as hourly Dst index but has the high time (i.e., 1 min) resolution. During the main phase of this storm, at least during the period from 1200 to 2400 UT, no AKR was detected in spite of the intense auroral electrojet activity with AL amplitudes less than  $-300$  nT, except for two transient AKR appearances at around 1200 UT and 1600 UT. Note that many solar type III radio bursts were recorded on the  $f$ - $t$  spectrogram, those are marked by the arrows on the top of the  $f$ - $t$  spectrogram. The absence of AKR during the main phase was an unexpected feature

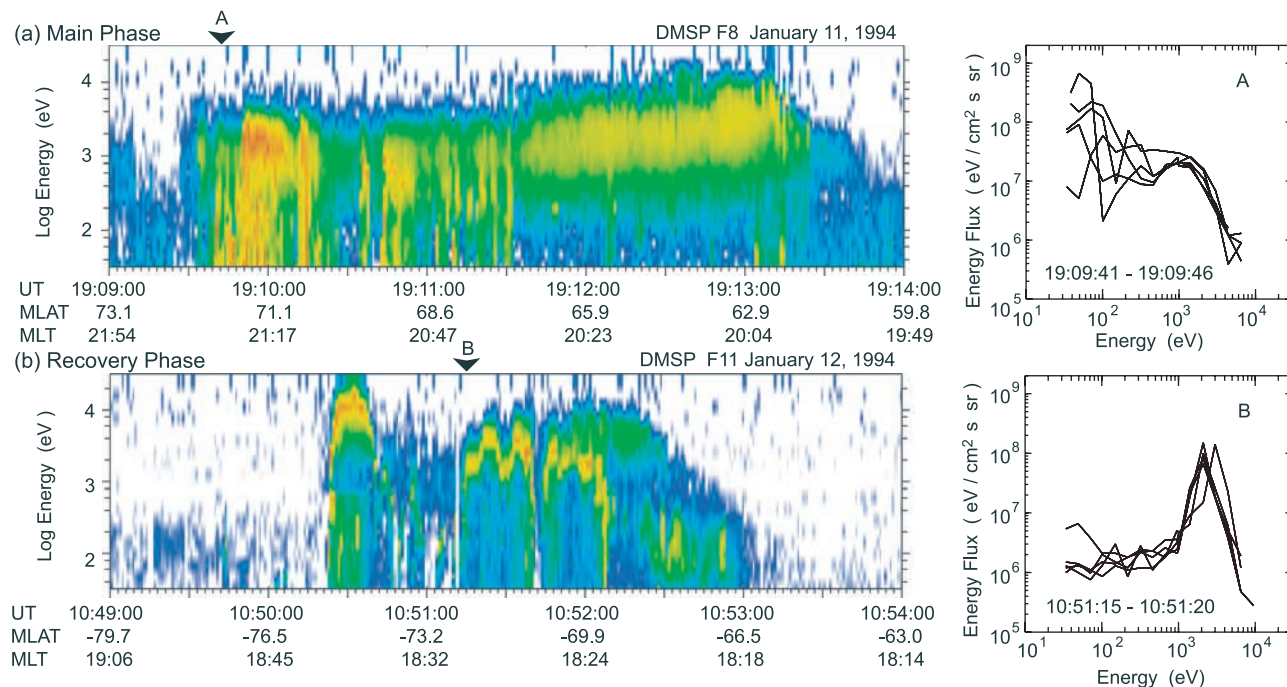


**Figure 2.** Energy-time ( $E$ - $t$ ) spectrogram of precipitating electrons in the energy range from 30 eV to 30 keV observed by DMSP satellite during (a) the main phase of 11 January storm and (b) the recovery phase. The time periods of Figures 2a and 2b correspond to those of the triangles in Figure 1. The upper right panel shows the superposed energy spectra for the period of 1909:41–1909:46 UT (corresponds to the triangle A in the left part). The lower right part shows the superposed energy spectra for the period of 1051:15–1051:20 UT (corresponds to the triangle B in the left part).

because the main phase was accompanied with violent auroral electrojet activity suggesting the development of field-aligned current probably driven by parallel electric fields in the M-I coupling region. From around 0000 UT on 12 January, corresponding to the end of the main phase, AKR appeared again with intense amplitudes in spite of relatively less auroral electrojet activity compared with that of the main phase.

[8] The disappearance and reappearance of AKR during 11 January storm were confirmed to be consistent with the radio wave observations by the Plasma Wave and Sounder Experiment (PWS) [Oya *et al.*, 1990] on board the Akebono satellite which was passing through the midnight auroral oval at the altitude of approximately 8300 km. The simultaneous precipitating electron spectrograms in the energy range from 30 eV to 30 keV observed in the duskside auroral region with the Precipitating Electron and Ion Spectrometer (SSJ/4) [Hardy *et al.*, 1984] on board the Defense Meteorological Satellite Program (DMSP) satellite are shown in Figure 2. The upper and lower left sides of the figure illustrate energy-time ( $E$ - $t$ ) spectrograms of electron energy flux during the main phase (Figure 2a from 1909 to 1914 UT on 11 January) and during the recovery phase (Figure 2b from 1049 to 1054 UT on 12 January). These two parts, Figures 2a and 2b, correspond to the times marked by triangles a and b at the lower side of the  $f$ - $t$  spectrogram in Figure 1. Superposed five energy spectra obtained for 5 s from 1909:41 to 1909:46 UT (triangle mark A in the upper left part) are shown in the upper right part and those obtained from 1051:15 to 1051:20 UT (triangle mark B in the lower left part) are in the lower right part. The

main phase spectrogram (Figure 2a) indicates an extremely wide storm-time auroral oval from magnetic latitude of  $63^\circ$  to  $72^\circ$ , and the energy range of the precipitation was remarkably broad in the dusk region. The 5-s energy spectra (upper right) did not show the features of the usual field-aligned acceleration in the dusk region but indicated hot electron precipitation in the energy range from 200 eV to 4 keV. The lower energy component below 200 eV showed very violent variations with time. These unusual precipitation spectra during the main phase were detected throughout the PSBL region from 1909:40 to 1911:30 UT. On the other hand, the energy spectra during the recovery phase (lower part) showed a well developed inverted V structure with a sharp energy peak. The width of the precipitation zone ( $67.5^\circ$ – $74^\circ$ ) was rather narrow compared with the main phase. The 5-s energy spectra indicate beam precipitation with a sharp energy peak at about 2 keV. These features of the storm-time precipitation are consistent with the report by Morioka *et al.* [2003].

[9] The hot electron injection was observed instead of beamed precipitation during the initial and main phase; this indicates that the field-aligned potential was very weak or not formed in the interaction region between the duskside magnetosphere and ionosphere. On the other hand, the AKR reappearance (AKR-on) and simultaneous beamed precipitation of electrons during the recovery phase indicate the reformation of the field-aligned potential.

[10] The current-voltage relation in the M-I coupling region was developed by Knight [1973] and discussed in detail by Lyons [1981]. The field-aligned current density is expressed, under the assumption that the current carrier is

the magnetospheric electrons with a Maxwellian distribution, as

$$j_{\parallel} = eN \left( \frac{K_{th}}{2\pi m_e} \right)^{\frac{1}{2}} \frac{B_i}{B_{V_{\parallel}}} \left[ 1 - \left( 1 - \frac{B_{V_{\parallel}}}{B_i} \right) \exp \left\{ - \frac{eV_{\parallel}}{K_{th} \left[ \left( \frac{B_i}{B_{V_{\parallel}}} \right) - 1 \right]} \right\} \right], \quad (1)$$

where  $j_{\parallel}$ ,  $N$ ,  $K_{th}$ , and  $V_{\parallel}$  are the field-aligned current density, plasma density, thermal energy, and field-aligned potential difference, respectively.  $B_i$  is the ionospheric magnetic field and  $B_{V_{\parallel}}$  is the magnetic field strength at the top of the potential variation along the field line. The  $e$  and  $m_e$  represent the electron charge and mass, respectively. Here, we consider that this current-voltage relation is valid even during magnetic storms. The case, where the field-aligned potential is not formed ( $V_{\parallel} = 0$ ) and AKR is “off” in spite of the heavy field-aligned current, implies that electrons with density  $N$  and thermal energy  $K_{th}$  are sufficiently supplied from the magnetosphere to maintain the field-aligned current in the magnetosphere-ionosphere coupling system. The case, where the field-aligned potential is reformed and AKR is “on” with the field-aligned current, suggests that the magnetospheric electron flux becomes insufficient to maintain the field-aligned current by itself, and then, the field-aligned potential is rebuilt so as to keep the necessary current-voltage relation in the system. From these considerations, we hypothesized that during the period of AKR-off, the plasma-sheet plasma shows some dense and/or hot state and that the plasma sheet plasma becomes the usual substorm state when AKR reappears. In the following, we examine the relationship between the AKR turn-on/turn-off and plasma sheet plasma density variation.

### 3. Storm Time AKR and Superdense Plasma Sheet

#### 3.1. Storm With AKR-Off

[11] Figure 3 shows another AKR disappearance phenomenon observed during a magnetic storm on 11–13 April 2001. The severe magnetic storm commenced at 1518 UT on 11 April 2001, and SYM-H index reached its minimum of  $-280$  nT at 2357 UT as seen in Figure 3b. Figure 3a illustrates AKR observed with the Radio Plasma Imager (RPI) [Reinisch *et al.*, 2000] on board the polar-orbiting IMAGE satellite. The low altitude and low  $L$  region ( $L < 5$ ) are masked by dark slits to hide the plasmaspheric wave phenomena. The arrows on the top of Figure 3a again indicate solar type III radio bursts.

[12] Before the magnetic storm commenced, AKR was active in the frequency range from 50 to 500 kHz. However, just after the storm commenced, the AKR intensity in the whole frequency range dropped to background level. During the main phase and early recovery phase of this storm, some violent storm-time substorms occurred with AL magnitudes of less than  $-1000$  nT. Nevertheless, AKR was not detected in this period. In the recovery phase of the storm at around 1100 UT on 12 April, AKR again appeared and continued for about 20 hours with intense amplitude. These disappearance and reappearance of AKR seen with the IMAGE satellite were also confirmed to be consistent with

the Geotail observation near the equatorial plane in the magnetosphere (not shown). Figures 3d and 3e represent the ion density and ion pressure in the energy range of 130 eV/q to 45 keV/q detected in the near-Earth plasma sheet as observed with the Los Alamos Magnetospheric Plasma Analyzer (MPA) [Bame *et al.*, 1993] on the 1994-084 geosynchronous satellite. The triangles indicate the local midnight of the satellite. The plasma sheet before the storm commenced exhibited a low plasma density of about  $0.6$ – $0.7$   $\text{cm}^{-3}$ , which is typical in the plasma sheet around the geosynchronous orbit [Thomsen *et al.*, 2003]. After the storm commenced, however, the plasma density steeply increased up to about  $5$   $\text{cm}^{-3}$  with violent fluctuations. This extremely high density in the plasma sheet has been denoted as “superdense plasma sheet” by Borovsky *et al.* [1997]. The density enhancement in the present case began to decrease from 0200 UT on 12 April and decayed to the preenhanced level at around 0800–1200 UT. It should be noted that the AKR disappearance took place during the period of this plasma enhancement and that the reappearance of AKR roughly coincided with the return of the plasma density to the normal level. The ion pressure in Figure 3e also indicated a significant increase showing almost parallel variation with that of the ion density. This superdense plasma feature at the time of AKR disappearance during the storm is also illustrated in Figure 1 where the bottom part of the figure indicates the ion density as detected by the MPA on the 1989-046 satellite. The sudden enhancement of the plasma sheet plasma density appeared at around 0600 UT when the substorm occurred with the AL amplitude of  $-400$  nT. Although the solar wind and IMF data are unfortunately not available for the day of interest, we suppose this timing may be the beginning of the magnetic storm or some large magnetospheric disturbance because it has been shown that the abrupt increases of plasma density at the synchronous orbit, as observed in the present case, are sometimes detected concurrent with the density jump of the solar wind [Borovsky *et al.*, 1997; Borovsky *et al.*, 1998; McComas *et al.*, 2002]. The speculation that the storm began at around 0600 UT on 11 January is also supported by evidence that the abnormal density enhancement of the solar wind was almost simultaneously developed at the distant tail of  $X = -90 R_E$  as detected with Low Energy Particle Experiment (LEP) [Mukai *et al.*, 1994] on board Geotail (not shown). Right after the recovery of the plasma density from enhanced to normal level at around 2200 UT, as shown in Figure 1, AKR was activated and continued throughout the recovery phase of the storm with intense power.

[13] These antirelations between AKR activity in the M-I coupling region and the density in the plasma sheet support the present hypothesis that the current carrier in the plasma sheet is sufficient to drive the field-aligned current during the early phase of a magnetic storm without field-aligned potential drop. Once the plasma sheet become unrich in the recovery phase, the field-aligned potential is built up to maintain the current-voltage relation between the magnetosphere and ionosphere resulting in the reradiation of AKR.

#### 3.2. Storm With Full-Time AKR

[14] As reported by Morioka *et al.* [2003], AKR disappearance is not always detected during magnetic storms.

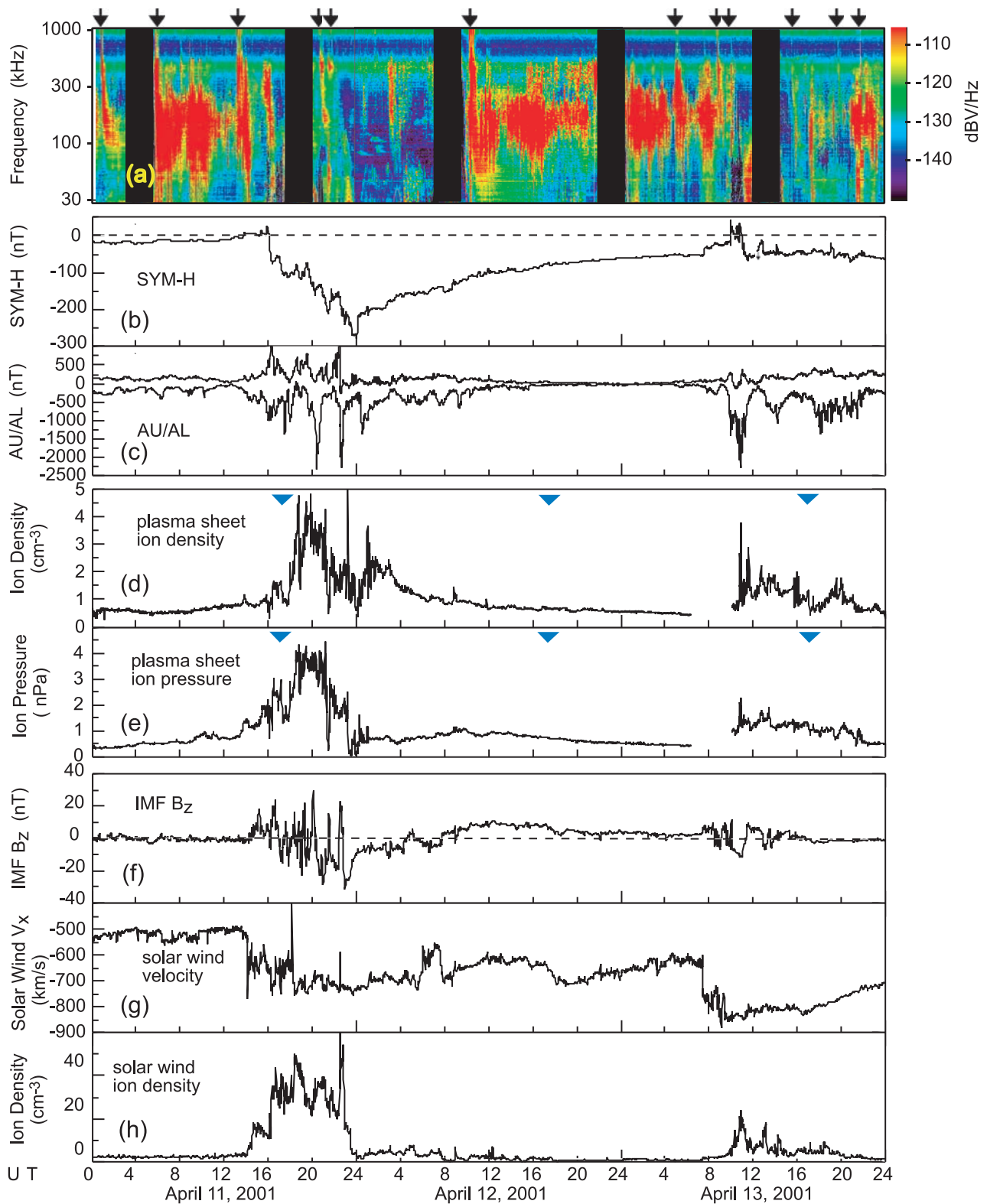


**Figure 3.** (a) The  $f-t$  spectrogram of radio waves in the frequency range from 30 to 1000 kHz observed with the PRI on board the IMAGE satellite during the 21 April 2001 storm. The black squares are the masks to hide the wave phenomena in the inner magnetosphere. The arrows on the top of the  $f-t$  spectrogram indicate the solar type III radio bursts. (b) SYM-H index. (c) AU and AL indices. (d) and (e) Plasma sheet ion density and plasma pressure in the energy range from 130 eV/q to 45 keV/q observed with the MPA on board the 1994-084 geosynchronous satellite. The triangles indicate the local midnight of the satellite. (f), (g), and (h) IMF  $B_z$ , solar wind velocity and solar wind ion density, respectively, observed by the WIND satellite.

Figure 4 shows the case where the AKR was stimulated immediately after the storm commenced and lasted throughout the initial and main phase of the storm. Here, we denote this type of storm as “storm with full-time AKR” and examine the relation between the storm with full-time AKR and plasma sheet density.

[15] The top of Figure 4 shows the AKR activity observed with Geotail during a magnetic storm on 17–18 February 1998. The AKR appeared around 1500 UT when the SYM-H polarity turned from positive to negative, that is, around the beginning of the main phase, and then AKR intensity increased as the storm proceeded. At around the minimum of SYM-H, AKR was strongly activated showing roughly concurrent variation with AL activity. Figures 4d and 4e again demonstrate the ion density and ion pressure at the geosynchronous orbit detected by MPA. The red and blue lines indicate data from the 1994-084 and LANL-97A satellites, respectively. The ion density became approximately twofold at the beginning of the storm and the increased density of about  $1.0 \text{ cm}^{-3}$  on average remained almost constant during the storm. The ion pressure (Figure 4e) also showed a small increase compared with the AKR disappearance phenomena in Figures 1 and 3 and maintained roughly constant pressure of about 1.5 nPa.

[16] From these analyses, we can say that magnetic storms that accompany full-time AKR do not exhibit the superdense plasma sheet but show a weak increase in both ion density and ion pressure in the plasma sheet. The occurrence of full-time AKR would signify the existence of the field-aligned potential drop between the ionosphere and magnetosphere throughout the storm. This situation is considered to be rather close to the usual substorm.

[17] Figure 5 shows the example of a typical substorm on 28 January 1997. The format of Figures 5a–5e is same as Figures 3 and 4. The typical AKR enhancement was detected simultaneously with the substorm onset at about 0315 UT and showed approximately concurrent variations with that of the auroral electrojet, as has been first demonstrated by Gurnett [1974]. During this typical substorm, the ion density and pressure in the plasma sheet did not show any particular change, as illustrated in Figures 5d and 5e. This can be understood from the current-voltage relation that substorms require the development of the field-aligned potential to establish the current circuit between magnetosphere and ionosphere.

#### 4. Solar Wind Condition and Storm-Time AKR

[18] In the previous section we described two types of magnetic storms in terms of association with AKR, that is, storms with AKR-off and storms with full-time AKR. In this section we examine the relation between storm-time AKR and interplanetary conditions. In Figures 3f, 3g, and 3h, the  $z$ -component of interplanetary magnetic field,  $B_z$ , observed with the Magnetic Field Investigation (MFI) [Lepping *et al.*, 1995] on board WIND spacecraft and solar wind velocity and density observed with the Solar Wind Experiment (SWE) [Ogilvie *et al.*, 1995] on WIND are illustrated. The sudden increase of both the solar wind velocity and density at WIND at 1410 UT caused a severe magnetic storm in the Earth’s magnetosphere. The interplanetary magnetic field  $B_z$  showed large amplitude

variations at the time of arrival and then exhibited a north to south variation and then south to north variation during the period from 1400 UT on 11 April to 2000 UT on 12 April. These magnetic field variations are an aspect of the interplanetary coronal mass ejection (ICME) and indicate the passage of the sheath region behind the shock and the magnetic cloud [e.g., Gonzalez *et al.*, 2001, 2002, and references there in]. During the passage of the ICME sheath region, the plasma density in the solar wind showed an unusual increase up to  $49.9 \text{ cm}^{-3}$  indicating the shock compression. This solar wind phenomenon at the WIND has been confirmed to be the full halo type CME with an expansion speed of  $2700 \text{ km s}^{-1}$  near the Sun [Dal Lago *et al.*, 2004]. By looking at the plasma-sheet plasma in Figures 3d and 3e, we can see that the rise of the superdense plasma in the plasma sheet followed an intense variation of the thick solar wind density with some delay. The delay would indicate the magnetospheric response to the CME passage, as has been investigated by Borovsky *et al.* [1998] and Thomsen *et al.* [1998]. As the first half of the magnetic cloud passed through the magnetosphere, the plasma density in the plasma sheet decreased to the prestorm level and then AKR reappeared. Note that the second jump of the solar wind velocity with rather small-scale magnetic field disturbance arrived at about 0800 UT on 13 April. This may be a high-speed stream with a shock following the magnetic cloud [Lepping *et al.*, 1997; Tsurutani *et al.*, 1999; Dal Lago *et al.*, 2001; Gonzalez *et al.*, 2002]. Associated with this interplanetary disturbance, the plasma density enhancement in the plasma sheet and AKR disappearance were again simultaneously detected. These evidences suggest that the buildup of the superdense plasma sheet is caused by the arrival of CME type solar wind disturbances and that the superdense plasma sheet causes the AKR-off in the M-I coupling region.

[19] The solar wind conditions at the time of a storm with full-time AKR are shown in Figures 4f, 4g, and 4h. The format is same as in Figure 3. In this case, the interplanetary magnetic field was characterized by a long-lasting negative  $B_z$  component for approximately 22 hours from 1100 UT on 17 February to 0900 UT on 18 February. The main phase of the magnetic storm began after the gradual turning of the interplanetary  $B_z$  from north to south, and the minimum SYM-H of  $-120 \text{ nT}$  was attained at around the time of minimum  $B_z$ . During the storm, the solar wind velocity was almost constant at about  $400 \text{ km s}^{-1}$  and plasma density showed a relatively high value of about  $10\text{--}20 \text{ cm}^{-3}$  with insignificant variations. In this case, no substantial relationship between the solar wind plasma density and plasma-sheet plasma was observed, as can be seen in Figures 4d and 4e. This suggests that a magnetic storm without significant plasma sheet density enhancement accompanies the full-time AKR.

#### 5. Summary and Conclusions

[20] Auroral kilometric radiation sometimes disappears (AKR-off) in the early phase of a magnetic storm and reradiates in the recovery phase. These AKR behaviors during magnetic storms were studied in terms of the current-voltage relation between the magnetosphere and ionosphere.

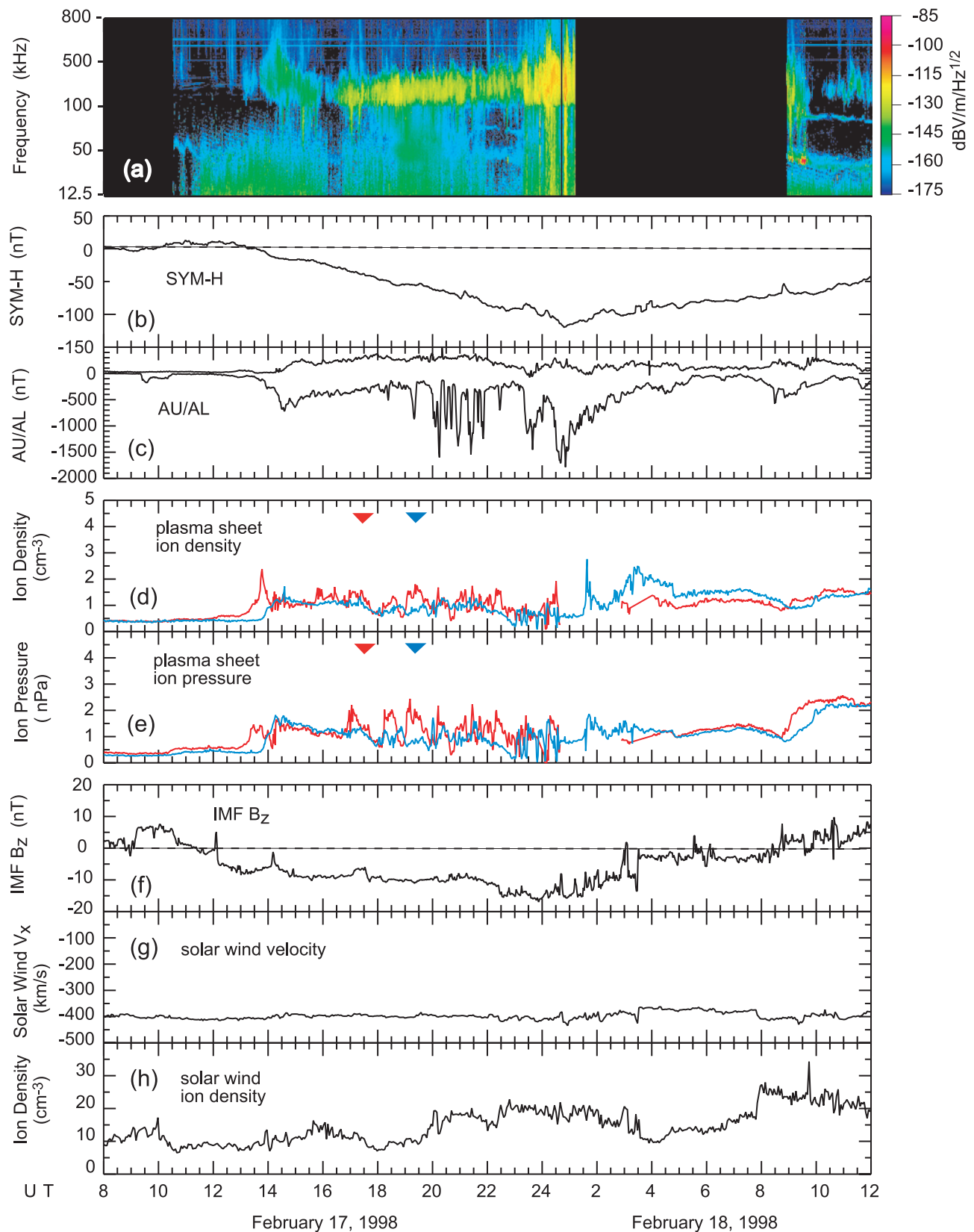


**Figure 4.** Same format as Figure 3 but Figure 4a was observed by Geotail in the frequency range of 12.5–800 kHz during the 17 February 1998 storm. The red and blue lines in Figures 4d and 4e indicate the data from 1994-084 and LANL-97A satellites, respectively. The triangles in the panels indicate the midnight of the satellites.

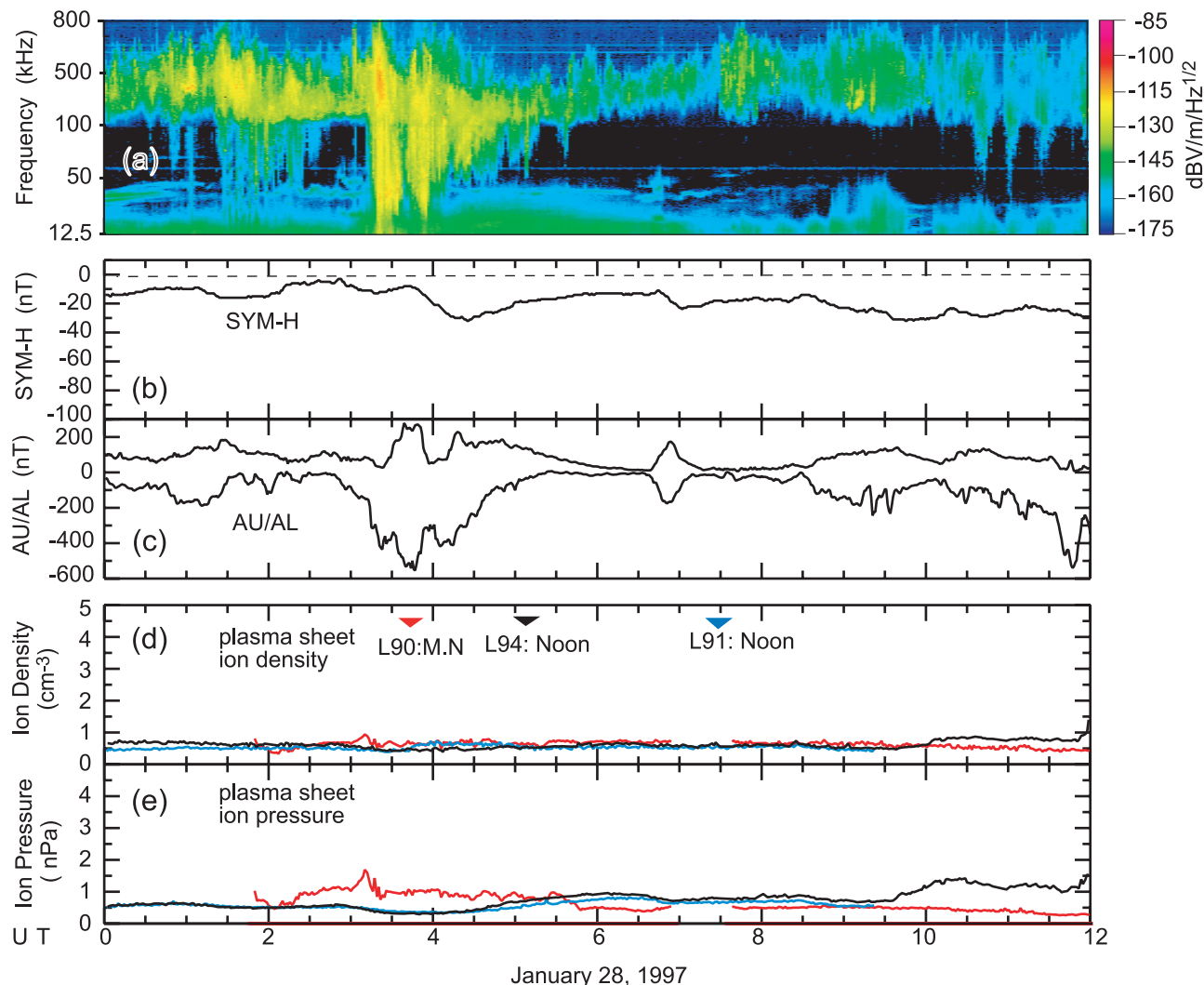


**Figure 5.** Same format as Figures 3a to 3e but observed by Geotail in the frequency range of 12.5–800 kHz during the 28 January 1997 substorm. The red, blue, and black lines in Figures 5d and 5e indicate the data from 1990-095, 1991-080, and 1994-084, respectively. The red triangle in Figures 5d and 5e shows the local midnight of 1990-095, and the blue and black triangles indicate the local noon of 1991-080 and 1994-084.

[21] The AKR-off state during the early phase of a magnetic storm was not associated with the usual inverted-V precipitation in the duskside M-I coupling region but rather with the intense hot electron precipitation. The energy spectrum of precipitating electrons during the period showed a nonaccelerated Maxwellian-type spectrum with a round spectral peak at around 1 keV. On the other hand, reradiated AKR in the recovery phase accompanied the typical inverted-V precipitation indicating well-developed field-aligned potential in the M-I coupling region. These observations confirm that AKR is radiated only by the beamed electrons accelerated by the field-aligned potential and is never radiated by the Maxwellian-type distribution of precipitating electrons. The Maxwellian-type spectrum observed during the early phase of the magnetic storm (upper right in Figure 2) is similar to the plasma sheet electrons, as has been observed by ISEE 1 [e.g., Eastman *et al.*, 1984; Christon *et al.*, 1988], suggesting that the electrons are injected from the plasma sheet.

[22] The statistical relationship between AKR power and magnetic activity has been investigated by Voots *et al.* [1977] and Murata *et al.* [1997]. Although their results showed that the AKR power generally enhances as the magnetic activity increases, the report by Murata *et al.* [1997] indicated that AKR power becomes to have no relation or rather negative correlation with Dst index when Dst index is less than  $-50$  nT. This statistical result may be consistent with that the magnetic storm has two types, storm with full-time AKR and storm with AKR-off.

[23] In spite of the absence of the field-aligned potential, the auroral electrojet was well developed during the storm-time substorm in the initial and main phase. This indicates that the upward field-aligned currents in the duskside M-I coupling region are maintained by the abundant current carrier directly injected from the plasma sheet, and hence developing the field-aligned potential was not necessary. This situation corresponds to the case when the magnetospheric plasma density  $N$  with thermal energy  $K_{th}$  are

reinforced in Knight's equation (equation (1)), whereas the field aligned potential  $V_{\parallel}$  becomes null. We consider that the particular enhancement of  $N$  with  $K_{th}$  in the Knight's equation would correspond to the superdense plasma sheet that provides the sufficient current carrier for the M-I coupling during the storm-time substorm. The evidence for the almost concurrent occurrence of the superdense plasma sheet with AKR disappearance supports this idea. On the other hand, the recovery of the plasma-sheet plasma density from enhanced to normal level was roughly coincident with the start of the reradiation of AKR. From this one can understand that the field-aligned potential was built up as the resources of the decreased current carrier in the plasma sheet. Not exact, but roughly, concurrence of AKR reradiation with the decline of the superdense plasma sheet, as seen in Figures 1 and 3, may be due to the spatial difference between the field-aligned current region in the plasma sheet and the in situ observation site of the magnetospheric plasma.

[24] To reinforce the current carrier in the plasma sheet, an abundant supply of hot plasma must be transferred into the plasma sheet from the outside. Borovsky *et al.* [1997, 1998] studied the relationship between the plasma-sheet plasma and solar wind in detail using the midtail and near-Earth plasma sheet data. Their statistical results showed that the plasma-sheet plasma density is strongly correlated with solar wind plasma density, and the plasma temperature of the plasma sheet is strongly correlated with the solar wind velocity. They also showed that the time lag between the arrival of the dense solar wind and the enhancement of plasma sheet density at the synchronous orbit is distributed between 0 and 7 hours. As for the consequence of the superdense plasma sheets, Borovsky *et al.* [1997] argued that the dense plasma sheet probably alters the dynamics of the magnetotail and changes the storm-time substorm during the period of the enhanced plasma density, which corresponds to the first day of a storm. They also discussed the possible stronger auroral current driven by the plasma sheet. The present argument is quite consistent with these studies and discussions. The enhanced polar wind outflow in the cleft region in response to the CME has been reported [e.g., Moore *et al.*, 1999]. This mass flow into the magnetospheric lobe may become a source of the superdense plasma sheet if the ejected plasma can be sufficiently heated up to  $\sim$ keV as the case of the superdense plasma sheet.

[25] The AKR disappearance phenomena during the magnetic storms can be explained by the following scenario. The CME with magnetic cloud provides the dense and hot solar wind plasma into the magnetosphere through the mantle [e.g., Pilipp and Morfill, 1976] and/or through the low-latitude boundary layer [e.g., Skopke *et al.*, 1981; Fujimoto *et al.*, 1998]. The efficiency of the plasma entry into the magnetosphere is increased for the period of the negative polarity of the  $B_Z$  in the ICME. During the relatively prolonged  $B_Z < 0$  period, the magnetospheric convection is also enhanced, and the efficient plasma transport results in the deep entry of the solar wind plasma into the near-Earth plasma sheet. The enriched plasma sheet can supply the sufficient current carrier for the field-aligned current in the M-I coupling system. The field-aligned current with sufficient carrier density can satisfy the necessary current-voltage relation between the magne-

tosphere and ionosphere without field-aligned acceleration. Thus the field-aligned potential is not built up, and as a consequence, AKR is not radiated. As the magnetic cloud passes by the Earth, the solar wind  $B_Z$  turns to positive and the solar wind plasma begins to decrease to the normal level. Accordingly, the reconnection rate decreases and the penetration of the solar wind plasma into the magnetosphere subsides, resulting in the reduction of the plasma-sheet plasma density. Then, the plasma sheet can no longer maintain the storm-time field-aligned current in the M-I coupling region by itself. As a consequence, field-aligned potential is built up and AKR is reradiated.

[26] **Acknowledgments.** We would like to thank M. Thomsen and J. Green for their useful comments. We are grateful to A. Kumamoto and M. Sato for their data processing of AKR observations. The IMAGE RPI data was kindly provided by J. Green and IMAGE/RPI data processing team. The DMSP spectrogram data and detailed ASCII data were available from the Auroral Particles and Imagery Group at The Johns Hopkins University Applied Physics Laboratory (JHU/APL). The solar wind and IMF data measured by WIND were provided by K. Ogilvie and R. Lepping at NASA through CDAWeb. The Auroral indices (AU and AL) and SYM-H data were obtained from the WDC-2 for Geomagnetism at Kyoto University, Japan. The LANL satellite data were kindly provided by M. Thomsen at Los Alamos National Laboratory though CDAWeb. This work was supported by a grant-in aid for scientific research (12440129) from the Ministry of Education, Science, Sports and Culture, Japan.

[27] Arthur Richmond thanks James L. Green and Jan Hanasz for their assistance in evaluating this paper.

## References

- Bame, S. J., et al. (1993), Magnetospheric plasma analyzer for spacecraft with constrained resources, *Rev. Sci. Instrum.*, *64*, 1026–1033.
- Borovsky, J. E., M. F. Thomsen, and D. J. McCormas (1997), The super dense plasma sheet: Plasmaspheric origin, solar wind origin, or ionospheric origin?, *J. Geophys. Res.*, *102*, 22,089–22,097.
- Borovsky, J. E., M. F. Thomsen, and R. C. Elphic (1998), The driving of the plasma sheet by the solar wind, *J. Geophys. Res.*, *103*, 17,617–17,639.
- Christon, S. P., D. G. Mitchell, D. J. Williams, L. A. Frank, C. Y. Huang, and T. E. Eastman (1988), Energy spectra of plasma sheet ions and electrons from  $\sim$ 50 eV/e to  $\sim$ 1 MeV during plasma temperature transitions, *J. Geophys. Res.*, *93*, 2562–2572.
- Dal Lago, A., W. D. Gonzalez, A. L. Clúa de Gonzalez, and L. E. A. Vieira (2001), Compression of magnetic clouds in interplanetary space and increase in their geoeffectiveness, *J. Atmos. Sol. Terr. Phys.*, *63*, 451–455.
- Dal Lago, A., L. E. A. Vieira, E. Echer, W. D. Gonzalez, A. L. Clua-Gonzalez, R. L. Guarnieri, L. Balmaceda, J. Santos, M. R. da Silva, and A. de Lucas (2004), Great geomagnetic storms in the rise and maximum of Solar Cycle 23, *Braz. J. Phys.*, *34*, 1542–1548.
- Eastman, T. E., L. A. Frank, W. K. Peterson, and W. Lennartsson (1984), The plasma sheet boundary layer, *J. Geophys. Res.*, *89*, 1553–1572.
- Fujimoto, M., T. Terasawa, T. Mukai, Y. Saito, T. Yamamoto, and S. Kokubun (1998), Plasma entry from the flanks of the near-Earth magnetotail: Geotail observations, *J. Geophys. Res.*, *103*, 4391–4408.
- Gonzalez, W. D., A. L. Clúa de Gonzalez, J. H. A. Sobral, A. Dal Lago, and L. E. Vieira (2001), Solar and interplanetary causes of very intense geomagnetic storms, *J. Atmos. Sol. Terr. Phys.*, *63*, 403–412.
- Gonzalez, W. D., B. T. Tsurutani, R. P. Lepping, and R. Schwnee (2002), Interplanetary phenomena associated with very intense geomagnetic storms, *J. Atmos. Sol. Terr. Phys.*, *63*, 173–181.
- Green, J. L., S. Boardsen, L. Garcia, S. F. Fung, and B. W. Reinisch (2004), Seasonal and solar cycle dynamics of the auroral kilometric radiation source region, *J. Geophys. Res.*, *109*, A05223, doi:10.1029/2003JA010311.
- Gurnett, D. A. (1974), The earth as a radio source: Terrestrial kilometric radiation, *J. Geophys. Res.*, *79*, 4227–4238.
- Gurnett, D. A., R. R. Anderson, F. L. Scarf, R. W. Fredricks, and E. J. Smith (1978), Initial results from the ISEE-1 and 2 plasma wave investigation, *Space Sci. Rev.*, *23*, 103–122.
- Hanasz, J., H. de Feraudy, R. Schreiber, G. Parks, M. Brittnacher, M. M. Mogilevsky, and T. V. Romantsova (2001), Wideband bursts of auroral kilometric radiation and their association with UV auroral bulges, *J. Geophys. Res.*, *106*, 3859–3871.

- Hardy, D. A., H. C. Yeh, L. K. Schmitt, T. L. Schumaker, M. S. Gussenhoven, A. Huber, F. J. Marshall, and J. Pantazis (1984), Precipitating electron and ion detectors (SSJ/4) on the block 5D/Flight 6-10 DMSP satellite: Calibration and data presentation, *Tech. Rep. AFGL-TR-84-0317*, Air Force Geophys. Lab., Hanscom Air Force Base, Mass.
- Kaiser, M. L., and J. K. Alexander (1977), Relationship between auroral substorms and the occurrence of terrestrial kilometric radiation, *J. Geophys. Res.*, *82*, 5238–5286.
- Kasaba, Y., H. Matsumoto, K. Hashimoto, and R. R. Anderson (1997), The angular distribution of auroral kilometric radiation observed by GEOTAIL spacecraft, *Geophys. Res. Lett.*, *24*, 2483–2486.
- Knight, S. (1973), Parallel electric fields, *Planet. Space Sci.*, *21*, 741–750.
- Kumamoto, A., and H. Oya (1998), Asymmetry of occurrence-frequency and intensity of AKR between summer polar region and winter polar region sources, *Geophys. Res. Lett.*, *25*, 2369–2372.
- Kumamoto, A., T. Ono, M. Iizima, and H. Oya (2003), Seasonal and solar cycle variation of the vertical distribution of the occurrence probability of auroral kilometric radiation sources and of upflowing ion events, *J. Geophys. Res.*, *108*(A1), 1032, doi:10.1029/2002JA009522.
- Lepping, R. P., et al. (1995), The WIND magnetic field investigation, *Space Sci. Rev.*, *71*, 207.
- Lepping, R. P., et al. (1997), The Wind magnetic cloud and events of October 18–20, 1995: Interplanetary properties and as triggers for geomagnetic activity, *J. Geophys. Res.*, *102*, 14,049–14,063.
- Lyons, L. R. (1981), The field-aligned current versus electric potential relation and auroral electrodynamics, *Physics of Auroral Arc Formation*, *Geophys. Monogr. Ser.*, vol. 25, edited by S.-I. Akasofu and J. R. Kan, pp. 252–259, AGU, Washington, D. C.
- Matsumoto, H., I. Nagano, R. R. Anderson, H. Kojima, K. Hashimoto, M. Tsutsui, T. Okada, I. Kimura, Y. Omura, and M. Okada (1994), Plasma wave observations with GEOTAIL spacecraft, *J. Geomagn. Geoelectr.*, *46*, 59–95.
- McComas, D. J., P. Valek, J. L. Burch, and C. J. Pollock (2002), Filling and emptying of the plasma sheet: Remote observations with 1–70 keV energetic neutral atoms, *Geophys. Res. Lett.*, *29*(22), 2079, doi:10.1029/2002GL016153.
- Menietti, J. D., A. M. Persoon, J. S. Pickett, and D. A. Gurnett (2000), Statistical study of kilometric radiation fine structure striations observed by Polar, *J. Geophys. Res.*, *105*, 18,857–18,866.
- Moore, T. E., W. K. Peterson, C. T. Russell, M. O. Chandler, M. R. Collier, H. L. Collin, P. D. Craven, R. Fitzenreiter, B. L. Giles, and C. J. Pollock (1999), Ionospheric mass ejection in response to a CME, *Geophys. Res. Lett.*, *26*, 2339–2342.
- Morioka, A., H. Oya, and S. Miyatake (1981), Terrestrial kilometric radiation observed by satellite Jikiken (Exos-B), *J. Geomagn. Geoelectr.*, *33*, 37–62.
- Morioka, A., et al. (2003), AKR disappearance during magnetic storms, *J. Geophys. Res.*, *108*(A6), 1226, doi:10.1029/2002JA009796.
- Mukai, T., S. Machida, Y. Saito, M. Hirahara, T. Terasawa, N. Kaya, T. Obara, M. Ejiri, and A. Nishida (1994), The low energy particle (LEP) experiment onboard Geotail satellite, *J. Geomagn. Geoelectr.*, *46*, 669–692.
- Murata, T., H. Matsumoto, H. Kojima, and T. Iyemori (1997), Correlations of auroral kilometric radiation index with Kp and Dst indices, *Proc. NIPR Symp. Upper Atmos. Phys.*, *10*, 64–68.
- Ogilvie, K. W., et al. (1995), SWE, a comprehensive plasma instrument for the WIND spacecraft, *Space Sci. Rev.*, *71*, 55–77.
- Oya, H., A. Morioka, K. Kobayashi, M. Iizima, T. Ono, H. Miyaoka, T. Okada, and T. Obata (1990), Plasma wave observation and stimulation experiments (PWS) using Akebono (EXOS-D) satellite instrumentation and initial results including discovery of the high altitude equatorial plasma turbulence, *J. Geomagn. Geoelectr.*, *42*, 411–442.
- Pilipp, W., and G. Morfill (1976), Plasma mantle as the origin of the plasma sheet, in *Magnetospheric Particles and Fields*, edited by B. M. McCormac, p. 55, Springer, New York.
- Pottelette, R., R. Tremann, and M. Berthomier (2001), Auroral plasma turbulence and the cause of auroral kilometric radiation fine structure, *J. Geophys. Res.*, *106*, 8465–8476.
- Reinisch, B. W., et al. (2000), The Radio Plasma Imager investigation on the IMAGE spacecraft, *Space Sci. Rev.*, *91*(2), 319–359.
- Sckopke, N., G. Paschmann, G. Haerendel, B. U. Ö. Sonnerup, S. J. Bame, T. G. Forbes, E. W. Hones Jr., and C. T. Russell (1981), Structure of the low-latitude boundary layer, *J. Geophys. Res.*, *86*, 2099–2110.
- Thomsen, M. F., J. E. Borovsky, D. J. McComas, R. C. Elphic, and S. Maurice (1998), The magnetospheric response to the CME passage of January 10–11, 1997, as seen at geosynchronous orbit, *Geophys. Res. Lett.*, *25*, 2545–2548.
- Thomsen, M. F., J. E. Borovsky, R. M. Skoug, and C. W. Smith (2003), Delivery of cold, dense plasma sheet material into the near-Earth region, *J. Geophys. Res.*, *108*(A4), 1151, doi:10.1029/2002JA009544.
- Tsurutani, B. T., Y. Kamide, W. D. Gonzalez, and R. P. Lepping (1999), Interplanetary causes of great and superintense magnetic storms, *Phys. Chem. Earth*, *24*, 101–105.
- Voots, G. R., D. A. Gurnett, and S.-I. Akasofu (1977), Auroral kilometric radiation as an indicator of auroral magnetic disturbances, *J. Geophys. Res.*, *82*, 2259–2266.
- W. Gonzalez, National Institute of Space Research, CP 515, 12201-970, São José dos Campos, SP, Brazil. (gonzalez@dge.inpe.br)
- K. Hashimoto and H. Matsumoto, Research Institute for Sustainable Humanosphere, Kyoto University, Gokanoshō, Uji, Kyoto 611-0011, Japan. (kozo@rish.kyoto-u.ac.jp; matsumot@rish.kyoto-u.ac.jp)
- H. Misawa, A. Morioka, T. Sakanoi, and F. Tsuchiya, Planetary Plasma and Atmospheric Research Center, Tohoku University, Sendai 980-8578, Japan. (misawa@pparc.geophys.tohoku.ac.jp; morioka@pparc.geophys.tohoku.ac.jp; tsakanoi@pparc.geophys.tohoku.ac.jp; tsuchiya@pparc.geophys.tohoku.ac.jp)
- Y. S. Miyoshi, Solar-Terrestrial Environment Laboratory, Nagoya University, Toyokawa 442-8507, Japan. (miyoshi@stelab.nagoya-u.ac.jp)
- T. Mukai and T. Seki, Institute of Space and Astronautical Science, Japan Aerospace Exploration Agency, Sagamihara, Kanagawa 229-8510, Japan. (mukai@stp.isas.jaxa.jp; seki@sirius.isas.jaxa.jp)
- H. Oya, Fukui University of Technology, Fukui 910-8505, Japan. (oya@cmail.fukui-ut.ac.jp)